

RESEARCH ARTICLE

Open Access



# Quantitative evaluation of mixed biomass burning and anthropogenic aerosols over the Indochina Peninsula using MERRA-2 reanalysis products validated by sky radiometer and MAX-DOAS observations

Takeru Ohno<sup>1\*</sup> , Hitoshi Irie<sup>1</sup>, Masahiro Momoi<sup>1,2,3</sup> and Arlindo M. da Silva<sup>4</sup>

## Abstract

In this study, we conducted the quantitative evaluation of aerosol optical properties in the Indochina Peninsula (ICP), which is significantly affected yearly by both biomass burning (BB) and anthropogenic aerosols, using Modern-Era Retrospective Analysis for Research and Applications, version 2 (MERRA-2) aerosol products. To perform spatiotemporal analysis with validated aerosol data, the MERRA-2 aerosol optical depth (AOD) and absorption AOD (AAOD) data were evaluated based on sky radiometer observations at the SKYNET Phimai site (15.18° N, 102.56° E). Furthermore, multi-axis differential optical absorption spectroscopy was conducted, providing additional data for the comparison of the aerosol extinction coefficient (AEC) vertical profile data. MERRA-2 AOD, AAOD, and AEC at altitudes below 1 km were underestimated in the dry season, with relative mean biases of 0.84, 0.54, and 0.48, respectively. These underestimations are attributed to insufficient BB emissions of light-absorbing aerosols near the surface. On the basis of these results, we investigated the factors that determined spatiotemporal variations in AOD over ICP from 2009 to 2020. We found that the seasonal variations in AOD were driven mainly by organic carbon (OC) and sulfate aerosols. OC AOD was dominant during the active BB period (from January to March), whereas sulfate AOD was high all year round, accounting for more than 25% of the total AOD. Sulfate AOD in the northeast ICP (NEIC) was approximately 74% of the total AOD in October, indicating the remarkable effect of sulfate aerosol transportation from southern China (SC). In the period of study, AOD decreased in NEIC and south ICP (SIC) by  $-4.40\%$  and  $-3.00\%$  year<sup>-1</sup>, respectively, corresponding to the decrease in sulfur dioxide concentrations in SC and NEIC. Thus, OC AOD was dominant during the active BB periods, whereas a significant amount of anthropogenic aerosols from SC contributed to the atmospheric environment over ICP throughout 2009–2020.

**Keywords:** Biomass burning, MERRA-2, Validation, AOD, Indochina Peninsula, Trend analysis

## 1 Introduction

Atmospheric aerosols affect the Earth's radiation budget and its climate system as they directly affect solar radiation and indirectly affect cloud characteristics. Aerosols produce a negative radiative forcing effect with considerable uncertainties (IPCC 2021). They also decrease air quality (Li et al. 2017b; Lee et al. 2017) and have adverse effects on human health, such as promoting lung cancer

\*Correspondence: t.ohno.chiba@gmail.com

<sup>1</sup> Center for Environmental Remote Sensing, Chiba University, 1-33 Yayoicho, Inage-Ku, Chiba 263-8522, Japan  
Full list of author information is available at the end of the article

and cardiovascular disease (Lave and Seskin 1970; Brook et al. 2010). There are various sources of aerosols, including anthropogenic sources (e.g., fossil fuel combustion) and natural sources (e.g., dust and sea salt particles) (Li et al. 2017a; Proestakis et al. 2018). Among the known sources, biomass burning (BB) is particularly important (van der Werf et al. 2006).

BB is the burning of living or dead vegetation. It is classified into anthropogenic (fuel and agricultural waste) and natural (lightning-induced) sources of aerosols. BB releases greenhouse gases, such as carbon dioxide, methane, and carbon monoxide. It also releases aerosols, such as black carbon (BC) and organic carbon (OC). BC and OC emitted from BB constitute 27% and 62% of the total global emissions, respectively (Wiedinmyer et al. 2011). BC absorbs light and exerts a warming effect on the globe. On the other hand, OC has a net cooling effect, although brown carbon absorbs sunlight in the ultraviolet (UV) and visible wavelength ranges (Ramanathan and Carmichael 2008; Bond et al. 2013). Several studies have estimated the direct radiative forcing of BrC, but the estimations have been weak in models ranging from +0.1 to +0.6  $\text{Wm}^{-2}$  (Wang et al. 2014; Lin et al. 2014; Brown et al. 2018). The optical properties of light-absorbing aerosols obtained from BB have not been clarified because their light absorption and scattering intensity vary with the type of combustion and atmospheric conditions (e.g., ambient temperature and relative humidity) (Dubovik et al. 2002; Vadrevu et al. 2015).

The Indochina Peninsula (ICP) is an active fire region, similar to Africa, Australia, and South America (van der Werf et al. 2017). The ICP has a dry season (October to May) and a wet season (June to September) because of its monsoon climate. In the dry season, BB occurs throughout the ICP, thereby causing seasonal variations in emissions (Yadav et al. 2017; Wang et al. 2015). There is a significant positive correlation between the monthly aerosol optical depth (AOD) and the number of monthly fire spots from December to May (Yin et al. 2019). Kalita et al. (2020) reported that carbonaceous AODs (OC and BC AODs) constitute 60% of the total AOD in the north ICP. In addition to BB, ICP is affected by anthropogenic aerosols. Analyses of direct air sampling at Phimai, Thailand, located at the central ICP, have shown that anthropogenic aerosols were transported from East Asia from October 2007 to March 2008 (Tsuruta et al. 2009). Besides, Kalita et al. (2020) and Hien et al. (2004) reported similar characteristics based on the assimilation of aerosol observations as well as the back-trajectory analysis, respectively. Therefore, ICP is affected by both BB and anthropogenic emissions. However, the contributions of various aerosols to AOD are complex; thus, quantitative analysis of aerosols in ICP is challenging.

In this study, we conducted the quantitative evaluation of aerosol optical properties in ICP, which is affected by both BB and anthropogenic aerosols, using the US National Aeronautics and Space Administration (NASA) Modern-Era Retrospective Analysis for Research and Applications, version 2 (MERRA-2) aerosol products. MERRA-2 employs state-of-the-art data assimilation techniques to determine the spatiotemporally homogeneous quality of aerosol data. To refine the evaluation for spatiotemporal analysis using MERRA-2 aerosol products, validation analysis was performed based on AOD and absorption AOD (AAOD) obtained using a sky radiometer and the aerosol extinction coefficient (AEC) obtained by multi-axis differential optical absorption spectroscopy (MAX-DOAS) at the SKYNET/Phimai site, Thailand. On the basis of the results, we analyzed the factors that determine spatiotemporal variations in AOD over ICP from 2009 to 2020.

## 2 Data and methods

### 2.1 Study area

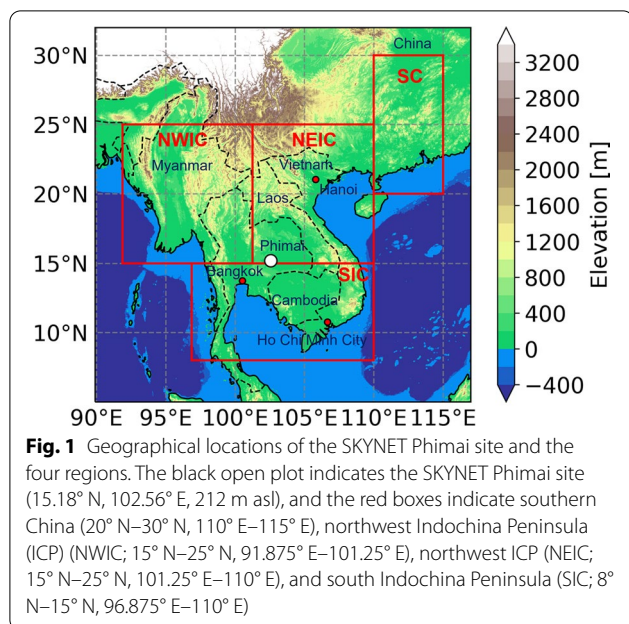
First, we validated MERRA-2 aerosol products based on ground-based observations obtained using a sky radiometer and MAX-DOAS at the SKYNET Phimai/Thailand site (15.18° N, 102.56° E; 212 m a.s.l.). The SKYNET Phimai site is located in central Thailand, approximately 270 km northeast of Bangkok. It is affected by the northeast and southeast monsoon during the dry (October to May) and wet (June to September) seasons, respectively.

We focused on southern China (SC; 20° N–30° N, 110° E–115° E) and three ICP regions for the spatiotemporal variability analysis (Fig. 1). According to the effects of BB and transboundary transport from China, ICP was divided into northwest ICP (NWIC; 15° N–25° N, 91.875° E–101.25° E), northeast ICP (NEIC; 15° N–25° N, 101.25° E–110° E), and south ICP (SIC; 8° N–15° N, 96.875° E–110° E).

### 2.2 Datasets

#### 2.2.1 Sky radiometer

Sky radiometer model POM-02 (Prede Co., Ltd., Japan) is a ground-based remote sensing instrument that measures direct and diffuse solar irradiances with a field of view of approximately 1° at 11 wavelengths over 10-min intervals. In this study, we used aerosol optical parameters, such as AOD and single scattering albedo (SSA), at 340, 380, 400, 500, 675, and 870 nm, retrieved using the Sky Radiometer analysis package of the Center for Environmental Remote Sensing (SR-CEReS) (e.g., Mok et al. 2018; Irie et al. 2019), which implements SKYRAD.pack version 5 (Hashimoto et al. 2012). SR-CEReS yielded homogeneous quality of aerosol optical property data by employing the



cross-improved Langley method as an onsite calibration to determine the calibration constant ( $F_0$ ) (Nakajima et al. 2020) and the solar disk scan method for the solid view angle (Nakajima et al. 1996; Uchiyama et al. 2018). Cloud screening was performed based on the Khatri and Takamura method (Khatri and Takamura 2009). The sky radiometer data retrieved by SR-CEReS were validated by comparing them with the Aerosol Robotic Network (AERONET), a multi-filter rotating shadow-band radiometer, and Pandora observations in Seoul, South Korea, during and after the Korea–US air quality field campaign in 2016 (Mok et al. 2018). Most AOD and SSA values were in good agreement, showing differences of  $\pm 0.01$  and  $\pm 0.05$ , respectively, at wavelengths of 340–870 nm.

The Ångström exponent (AE), AAOD, and absorption AE (AAE) were derived from the AOD and SSA at wavelengths of 340–870 nm. To modify the analysis, we selected data where the uncertainty in AAOD was less than the estimated propagation of error, and the linearity of  $\ln(\text{AAOD})$  versus  $\ln(\text{wavelength})$  was as high as expected (Irie et al. 2019). To validate MERRA-2 aerosol products at the same wavelength, the AOD obtained using the sky radiometer was interpolated to 550 nm using AE based on the following equation:

$$\tau_{550} = \tau_{500} \left( \frac{550}{500} \right)^{-\alpha}, \quad (1)$$

where  $\tau$  and  $\alpha$  represent AOD and AE, respectively. Similarly, AAOD was interpolated using AAE.

### 2.2.2 MAX-DOAS

The MAX-DOAS is a ground-based remote sensing instrument that measures UV–visible spectra of scattered sunlight at several elevation angles between the horizon and the zenith. MAX-DOAS retrieves the concentrations of various trace gases based on the Beer–Lambert law. Our MAX-DOAS instrument mainly consists of an outdoor telescope unit and an indoor spectrometer unit, containing the Maya2000 Pro UV–visible spectrometer (Ocean Insight, Inc.) with a slit of 25  $\mu\text{m}$ . Spectra at 310–515 nm were measured at a wavelength resolution of approximately 0.3–0.4 nm (as the full width at half maximum). Several scattered sunlight spectra were measured using five off-axis elevation angles (2°, 3°, 4°, 6°, and 8°) and a reference angle of 70° every 30 min (–November 7, 2016) and 15 min (November 8, 2016–).

For the retrieval, we used the Japanese MAX-DOAS profile retrieval algorithm, version 2 (JM2) (Irie et al. 2011, 2015, 2019). First, the wavelengths were calibrated daily to correct for possible wavelength shifts and determine the wavelength resolution as a function of wavelength. Then, nonlinear least-square spectral fitting (DOAS fitting) was performed to estimate the differential slant column density ( $\Delta\text{SCD}$ ), which is the difference between the SCDs of the reference and off-axis measurements, for oxygen collision complex ( $\text{O}_4$ ) and other trace gases, including  $\text{NO}_2$ ,  $\text{HCHO}$ ,  $\text{CHOCHO}$ ,  $\text{H}_2\text{O}$ ,  $\text{SO}_2$ , and  $\text{O}_3$ . Our spectrometer covered the absorption bands of  $\text{O}_4$  for both the UV and visible regions. From the determined  $\text{O}_4$   $\Delta\text{SCD}$ , lower-troposphere vertical profiles of AECs at 357 and 476 nm were retrieved using the optimal estimation method (Rodgers 2000). As revealed by the collocated sky radiometer, LIDAR, and cavity ring-down spectroscopy results, uncertainty in MAX-DOAS AEC data for a 0–1 km layer was less than 30% (e.g., Irie et al. 2008, 2015). The AEC from MAX-DOAS was interpolated to 532 nm using the AE value obtained using the sky radiometer within  $\pm 8$  min of the MAX-DOAS analysis (Eq. 1).

### 2.2.3 MERRA-2

MERRA-2 is the latest atmospheric and aerosol reanalysis product from NASA's Global Modeling and Assimilation Office (Gelaro et al. 2017). It is based on the Goddard Earth Observing System, version 5 (GEOS-5), with the Goddard Chemistry Aerosol Radiation and Transport model (GOCART; Chin et al. 2002) aerosol module (Randles et al. 2017; Buchard et al. 2017). The spatial resolution of MERRA-2 model is 0.5° latitude by 0.625° longitude with 72 layers from the surface to 0.01 hPa, and data are collected at intervals, ranging from hourly to annually. MERRA-2 AOD in the model is the

integration of the aerosol mixing ratio, extinction coefficient, and relative humidity. AOD is expressed as the sum of the AODs of five aerosols (BC, OC, dust, sea salt, and sulfate). Emissions in the GEOS-5/GOCART model vary among databases and temporal resolutions, depending on the aerosol type. For BB emissions, the Global Fire Emission Dataset version 3.1 from 1997 to 2009 and the Quick Fire Emissions Dataset version 2.4-r6 from 2009 were employed in the MERRA-2 model (van der Werf et al. 2006; Darmenov and da Silva 2015). Anthropogenic  $\text{SO}_2$ ,  $\text{SO}_4$ , and carbonaceous aerosols are covered until 2008. MERRA-2 assimilates bias- and non-bias-corrected AODs from observations (Burchard et al. 2017). Bias-corrected AOD observations are obtained using an advanced very-high-resolution radiometer (1980–2002) over the ocean and a Moderate-Resolution Imaging Spectroradiometer (MODIS) (Terra/Aqua satellite; 2000/2002 to present) under a <70% cloud cover. The non-bias-corrected AOD observations include the AERONET (1999–2014) stations and the multi-angle imaging spectroradiometer (Terra; 2000–2014) over bright surfaces (albedo > 0.15). MERRA-2 aerosol products are available at the NASA Goddard Earth Sciences Data and Information Services Center, but not for AEC products.

The MERRA-2 aerosol products have been validated at several sites by comparing them with ground-based observations, but such comparisons are limited to BB regions. MERRA-2 AOD results have shown a good spatial agreement with ground-based observations (Shi et al. 2019; Gueymard and Yang 2020), but the absolute values were underestimated in southeast Asia (Che et al. 2019). Because BB-originating plumes are primarily affected

by light-absorbing aerosols near the surface, AAOD and AEC are important for validating reanalysis data.

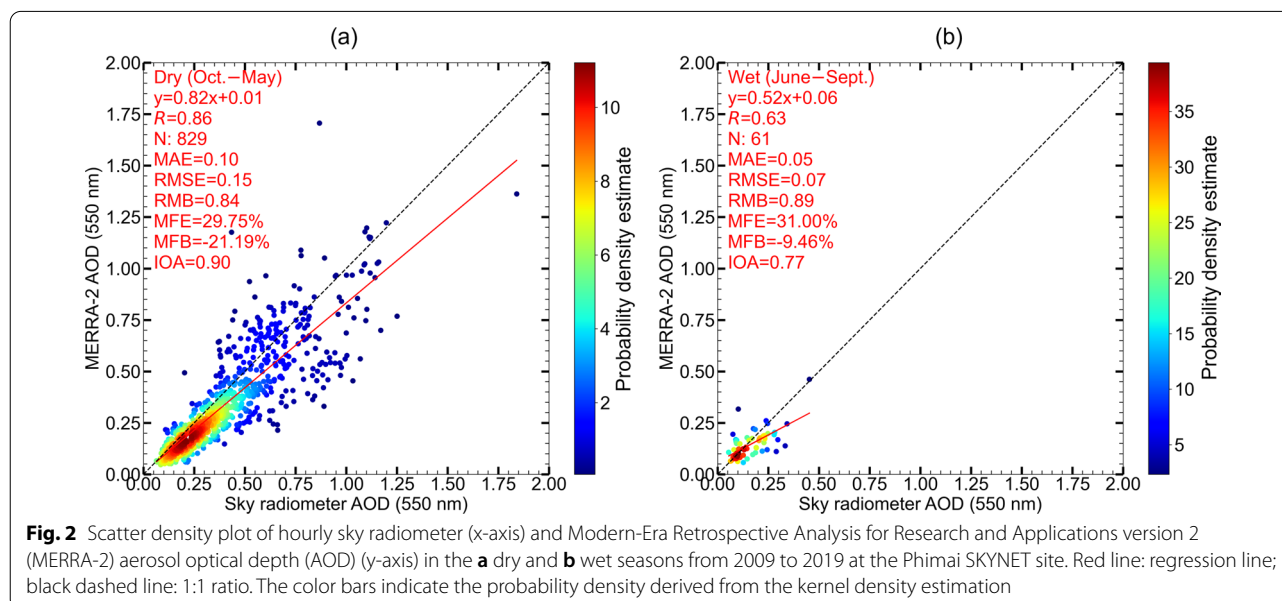
In this study, we used the hourly extinction AOD and scattering AOD (SAOD) data for total aerosols, BC, OC, dust, sea salt, and sulfate ('tavgl\_2d\_aer\_Nx'). AAOD was calculated by subtracting SAOD from the extinction AOD. The 3-hourly AEC was obtained from the model-estimated value constrained by column-integrated aerosol extinction (i.e., AOD). Notably, AAOD and AEC were obtained from model-estimated values, which were constrained by only AOD.

#### 2.2.4 MODIS

The MODIS Collection 6.1 AOD product was used to support the trend analysis (Levy et al. 2007; Wei et al. 2019). MODIS sensors are on board the Terra and Aqua satellites in the morning (10:30 local time) and afternoon (13:30 local time) orbits, respectively. Data were obtained in 36 spectral bands at 0.4–14  $\mu\text{m}$  with various parameters, such as aerosols, vegetation, and cloud. We used a spatial resolution of 10 km  $\times$  10 km AOD (550 nm) at 10:30 and 13:30 local time from 2009 to 2020. In the trend analysis, the monthly mean AOD was calculated for each region shown in Fig. 2. To reduce cloud-induced uncertainties, AOD at less than 20% cloud fraction was used.

#### 2.3 Validation approach

First, hourly MERRA-2 AOD was validated using sky radiometer data in the dry and wet seasons. In the dry season, light-absorbing aerosols emitted from BB cause uncertainties in the optical properties of the atmosphere,



especially near the surface. Thus, MERRA-2 AAOD in the dry season was validated using the sky radiometer, which is sensitive to UV wavelengths. Besides, AEC below 1 km from the MAX-DOAS data was used to validate MERRA-2 in the season. Considering the continuous data availability, we used sky radiometer data from 2009 to 2019 and MAX-DOAS data from 2014 to 2019. To exclude uncertainties in the observation data, we used data from 9:00 to 15:00 local time, and thresholds were set while calculating the averages. The hourly mean AOD and AAOD were calculated when three observation datasets existed per hour or more. Similarly, the hourly mean AEC was calculated when two observation datasets exist per hour or more. MERRA-2 aerosol products were validated using the slope of the regression line (hereafter, slope), Pearson correlation coefficient ( $R$ ), mean absolute error (MAE), root-mean-square error (RMSE), relative mean bias (RMB), mean fractional error (MFE), mean fractional bias (MFB) and index of agreement (IOA), as in previous studies (Yumimoto et al. 2017; Che et al. 2019):

$$\text{MAE} = \frac{1}{n} \sum_{i=1}^n |M_i - O_i|, \quad (2a)$$

$$\text{RMSE} = \sqrt{\frac{1}{n} \sum_{i=1}^n (M_i - O_i)^2}, \quad (2b)$$

$$\text{RMB} = \frac{\overline{M}}{\overline{O}}, \quad (2c)$$

$$\text{MFE} = \frac{2}{n} \sum_{i=1}^n \frac{|M_i - O_i|}{M_i + O_i} \times 100, \quad (2d)$$

$$\text{MFB} = \frac{2}{n} \sum_{i=1}^n \frac{M_i - O_i}{M_i + O_i} \times 100, \quad (2e)$$

$$\text{IOA} = 1 - \frac{\sum_{i=1}^n (O_i - M_i)^2}{\sum_{i=1}^n (|O_i - \overline{O}| + |M_i - \overline{M}|)^2}, \quad (2f)$$

where  $n$  is the total number of pairs of modeled ( $M$ , MERRA-2 AOD, AAOD, and AEC) and observed ( $O$ , sky radiometer AOD and AAOD, and MAX-DOAS AEC) values.  $\overline{M}$  and  $\overline{O}$  are the mean values of  $\{M_i\}$  and  $\{O_i\}$ , respectively, and MAE and RMSE the magnitudes of bias between MERRA-2 and observation values. RMB indicates the underestimation ( $\text{RMB} < 1$ ) or overestimation ( $\text{RMB} > 1$ ). MFE and MFB are indices that normalize the bias and error for each model and each observation by the observed value, respectively. MFE ranges from 0% to +200%, and MFB ranges from -200% to +200%. To evaluate the model performance, Boylan and Russell (2006) set model performance goals and criteria for

light extinction and particulate matter. The model performance goals include  $\text{MFE} \leq +50\%$  and  $\text{MFB} \leq \pm 30\%$ , and the model performance criteria are  $\text{MFE} \leq +75\%$  and  $\text{MFB} \leq \pm 60\%$ . IOA indicates the model accuracy and ranges from 0 to 1 (Willmott 1981), IOA = 1 indicating perfect model performance.

#### 2.4 Spatiotemporal variability analysis

In addition to MERRA-2 AOD, OC and sulfate AODs were used to quantitatively analyze the factors that contribute to the spatial and temporal variations in aerosols in ICP regions. NEIC is exposed to anthropogenic aerosols because Hanoi, Vietnam, and China are located in the northeast, and BB is high in the dry season. In contrast, BB is highest in NWIC, although NWIC is least affected by transboundary air pollution from China. BB begins earlier in SIC than in other regions (Lasko et al. 2019), and large cities, such as Bangkok in Thailand and Ho Chi Minh City in Vietnam are located in SIC. In this analysis, monthly AODs from 2009 to 2020 were calculated using hourly data. The trend analysis was conducted using the following equation:

$$\text{Trend} (\% \text{year}^{-1}) = \frac{\text{Slope}}{\mu} \times 100 \quad (3)$$

where slope is the slope of the regression line and  $\mu$  is the mean value for the period used in each dataset.

### 3 Results and discussion

#### 3.1 Validation of MERRA-2 aerosol products

##### 3.1.1 AOD

Sensitivity to wavelengths in the UV region is important for observing the optical properties of BrC, which has strong absorption in the UV region (Mok et al. 2016). UV SSA data retrieved from sky radiometer results are sensitive to BB plumes (Irie et al. 2019). Figure 2 shows the hourly MERRA-2 and sky radiometer AOD data at Phimai in dry and wet seasons. Most AOD values were smaller than 0.5, with significant seasonal variations, showing some AOD values larger than unity only in the dry seasons. Similar seasonal variations in AOD were reported by Sugimoto et al. (2015).

In dry seasons, MERRA-2 and sky radiometer AOD data have a significant positive correlation ( $R=0.86$ ; Fig. 2a), with MAE and RMSE of 0.10 and 0.15, respectively. The MFE and MFB values were 29.75% and -21.19%, both of which are within the goal criteria defined by Boylan and Russell (2006), indicating that MERRA-2 AOD data have an accuracy comparable to that expected for the best model. The IOA value was high at 0.90. As quantified with these statistical indices, the MERRA-2 AOD and sky radiometer data were in good agreement. In contrast, the slope and RMB were 0.82

and 0.84, respectively, indicating an underestimation of MERRA-2 AOD.

As shown in Fig. 2b, in the wet season, MERRA-2 and sky radiometer AOD data showed a moderate positive correlation, with an  $R$  of 0.63 but significant differences in the slope (0.52) and RMB (0.89). These differences may be attributed to the small number of datasets used for the validation in the wet seasons ( $N=61$ ), as data with cloud contaminations were excluded from the analysis. This indicates that only a few observations were assimilated by MERRA-2. The MAE and RMSE were 0.05 and 0.07, and the MFE and MFB were within the goal criteria (31.00% and  $-9.46\%$ , respectively). The IOA was high at 0.77. Despite the sparsity in the sky radiometer data, the accuracy of MERRA-2 was acceptable based on the statistical indices.

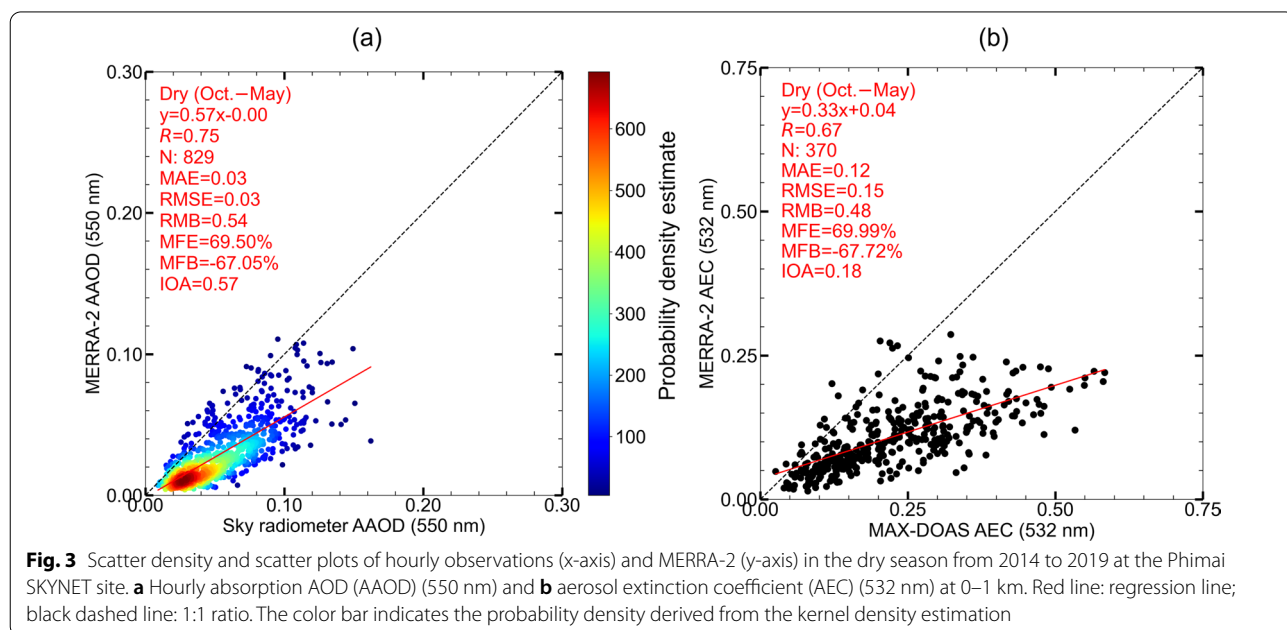
In the dry seasons, MERRA-2 AOD was underestimated based on the statistical indices compared with data from the sky radiometer, as discussed above. This is consistent with results obtained at the AERONET Phimai site (Che et al. 2019). Because the aerosol sources are complex, there are two possible reasons for the underestimation of MERRA-2 AOD: underestimation of anthropogenic aerosols or underestimation of BB aerosols. Although Sun et al. (2019a, b) reported the underestimation of MERRA-2 AOD over China because nitrate emissions are absent in the MERRA-2 model, the Phimai site is in a rural area and is geographically distant from the source of anthropogenic aerosol emissions (Bangkok or China). Thus, we presumed that the underestimation of AOD was more likely because BB activities are

strong during the dry season. Buchard et al. (2016, 2017) reported that the underestimation of OC emissions in the MERRA-2 model contributes to discrepancies in near-surface observations. Therefore, the underestimation of MERRA-2 AOD was likely attributed to the lack of BB aerosols, including OC and BC.

### 3.1.2 AAOD and AEC in the dry season

Figure 3A compares hourly MERRA-2 and sky radiometer AAOD data at Phimai in dry seasons. MERRA-2 and sky radiometer data are consistent, with an  $R$  of 0.75. The slope and RMB were 0.57 and 0.54, respectively. The MAE and RMSE were both 0.03, and the MFE and MFB were 69.50% and  $-67.05\%$ , respectively. These values exceed the criteria. The IOA value was low at 0.57. Therefore, MERRA-2 AAOD data at Phimai do not satisfy the criteria.

Figure 3b shows the MERRA-2 and MAX-DOAS AECs near the ground (below 1 km) at Phimai in the dry season. MERRA-2 data showed a moderate correlation with an  $R$  of 0.67. MERRA-2 underestimated AEC as the slope and RMB were 0.33 and 0.48, respectively. On the basis of the MFE, MFB, and IOA values, AEC was not estimated as accurate as AOD (Figs. 2a and 3b). In the MERRA-2 model, BB emissions are distributed uniformly throughout the planetary boundary layer (Randles et al. 2017). Because the MERRA-2 AEC depends on the vertical distribution of aerosols in the model, the discrepancy in the AECs near the ground is attributed to the lack of emissions near the ground or uncertainties in the emission injection height.



For the validations of both AAOD and AEC in the dry season, MERRA-2 was significantly underestimated, but AOD constraints may have resulted in a moderate correlation between AAOD and AEC since AAOD and AEC were calculated using the MERRA-2 model. These results indicate that, because of the light-absorbing BB emissions near the ground in the dry season at Phimai, MERRA-2 may underestimate the AOD.

### 3.1.3 Correction of MERRA-2 AOD at the Phimai site

MERRA-2 underestimated AOD in dry seasons, as discussed above; thus, we corrected it. Similar to the above-mentioned validation results for MERRA-2 AEC at altitudes below 1 km, the underestimation of OC emissions in the MERRA-2 model is attributed to the uncertainty in the surface aerosols (Buchard et al. 2017). BC aerosol has a small contribution to AOD but a large contribution to AAOD (Randles et al. 2016). Therefore, assuming OC and BC (light-absorbing aerosol from BB) are underestimated by MERRA-2, a correction factor was calculated to make MERRA-2 AOD equivalent to those obtained using the sky radiometer. We corrected the MERRA-2 AOD assuming that the underestimation of AOD was due to the underestimation of (1) only OC AOD or (2) both OC and BC AODs by the same amount. The correction factors were calculated as 1.35 for case 1 and 1.30 for case 2 using the following equations:

$$\tau_{total_1} = 1.35\tau_{OC} + \tau_{BC} + \tau_{dust} + \tau_{seasalt} + \tau_{sulfate}, \tag{4a}$$

$$\tau_{total_2} = 1.30\tau_{OC} + 1.30\tau_{BC} + \tau_{dust} + \tau_{seasalt} + \tau_{sulfate}, \tag{4b}$$

Table 1 lists the statistical metrics of the sky radiometer and the MERRA-2 AAOD and SAOD without the AOD correction, underestimation of OC AOD, and identical underestimation of OC and BC AOD at the Phimai SKYNET site. The biases (MAE and RMSE) of AAOD and SAOD with and without AOD correction are not significantly different. The slope and RMB of AAOD were improved from 0.57 to 0.74 and 0.54 to 0.70, respectively,

in the case 2 correction. In the dry season, the contribution of BC AAOD was high (mean, 88%). Thus, the case 2 correction improved the underestimation of AAOD compared to the case 1 correction. The slope and RMB of SAOD were improved to almost 1:1 in both cases of correction. Because the mean ratio of SAOD to AOD was 92%, correction for strong light-absorbing BC did not significantly influence the SAOD correction. The MFE and MFB of AAOD were improved to meet the criteria in the case 2 correction, and IOA was improved by 0.77. The improvement in these indices in the case 2 correction indicates that corrections for OC and BC can improve the MERRA-2 AAOD and SAOD at Phimai in the dry season.

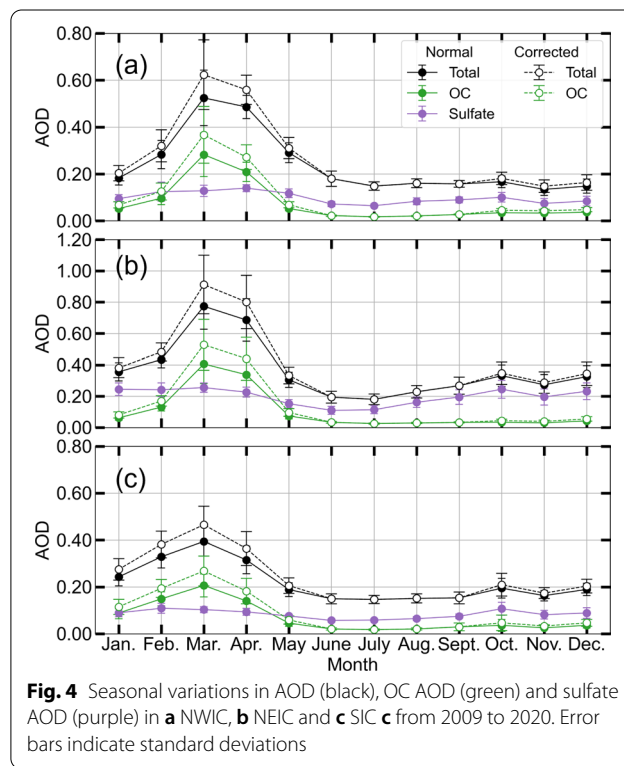


**Fig. 4** Seasonal variations in AOD (black), OC AOD (green) and sulfate AOD (purple) in **a** NWIC, **b** NEIC and **c** SIC **c** from 2009 to 2020. Error bars indicate standard deviations

**Table 1** Statistical metrics of AAOD and scattering AOD (SAOD) without AOD correction (normal), underestimation of OC AOD (case 1), and identical underestimation of OC and BC AOD (case 2) at the Phimai SKYNET site

	Correction	Slope	R	MAE	RSME	RMB	MFE	MFB	IOA
AAOD	Normal	0.57	0.751	0.025	0.030	0.54	69.49	-67.04	0.57
	Case 1	0.60	0.750	0.024	0.029	0.56	67.54	-64.48	0.61
	Case 2	0.74	0.750	0.020	0.025	0.70	53.22	-44.80	0.77
SAOD	Normal	0.82	0.844	0.088	0.132	0.89	27.10	-14.49	0.91
	Case-1	1.01	0.842	0.094	0.147	1.03	25.41	-2.88	0.91
	Case-2	0.99	0.843	0.092	0.144	1.01	25.35	-3.83	0.91

### 3.2 3.2 Seasonal variation

We analyzed factors that influence the AOD in NWIC, NEIC, and SIC based on the validated MERRA-2 AOD data. The major causes of seasonal variation are OC and sulfate aerosols (Kalita et al. 2020). Figure 4 shows seasonal variations in AOD, OC AOD, and sulfate AOD in NWIC, NEIC, and SIC from 2009 to 2020. The AODs in the regions were significantly higher in the dry season than in the wet season. The maximum AOD value in the dry season was higher in NWIC and NEIC than in SIC. BB occurs in the south, and the peak AOD moves north,

reaching a maximum in NWIC and NEIC (Lasko et al. 2019). This may explain the difference in AOD intensity between the northern region and SIC. In this study, for all regions, OC AODs were dominant from February to April and constituted more than 50% of the total AOD in March. In contrast, the sulfate AOD accounted for more than 25% all year round. Besides, small AOD peaks in NEIC and SIC were observed in October, during which AOD in NEIC was strongly influenced by sulfate aerosol, accounting for approximately 74% of the total AOD.

**Table 2** Changes in the OC and sulfate AOD ratios before and after correction in the dry season

Region	Species	Jan (%)	Feb (%)	Mar (%)	Apr (%)	May (%)	Oct (%)	Nov (%)	Dec (%)
NWIC	OC	16	15	9	13	22	20	18	18
	Sulfate	-10	-12	-16	-13	-6	-8	-9	-9
NEIC	OC	21	17	10	11	19	24	24	23
	Sulfate	-7	-10	-15	-14	-8	-5	-5	-6
SIC	OC	15	12	10	13	19	21	22	21
	Sulfate	-12	-14	-15	-13	-8	-7	-6	-7

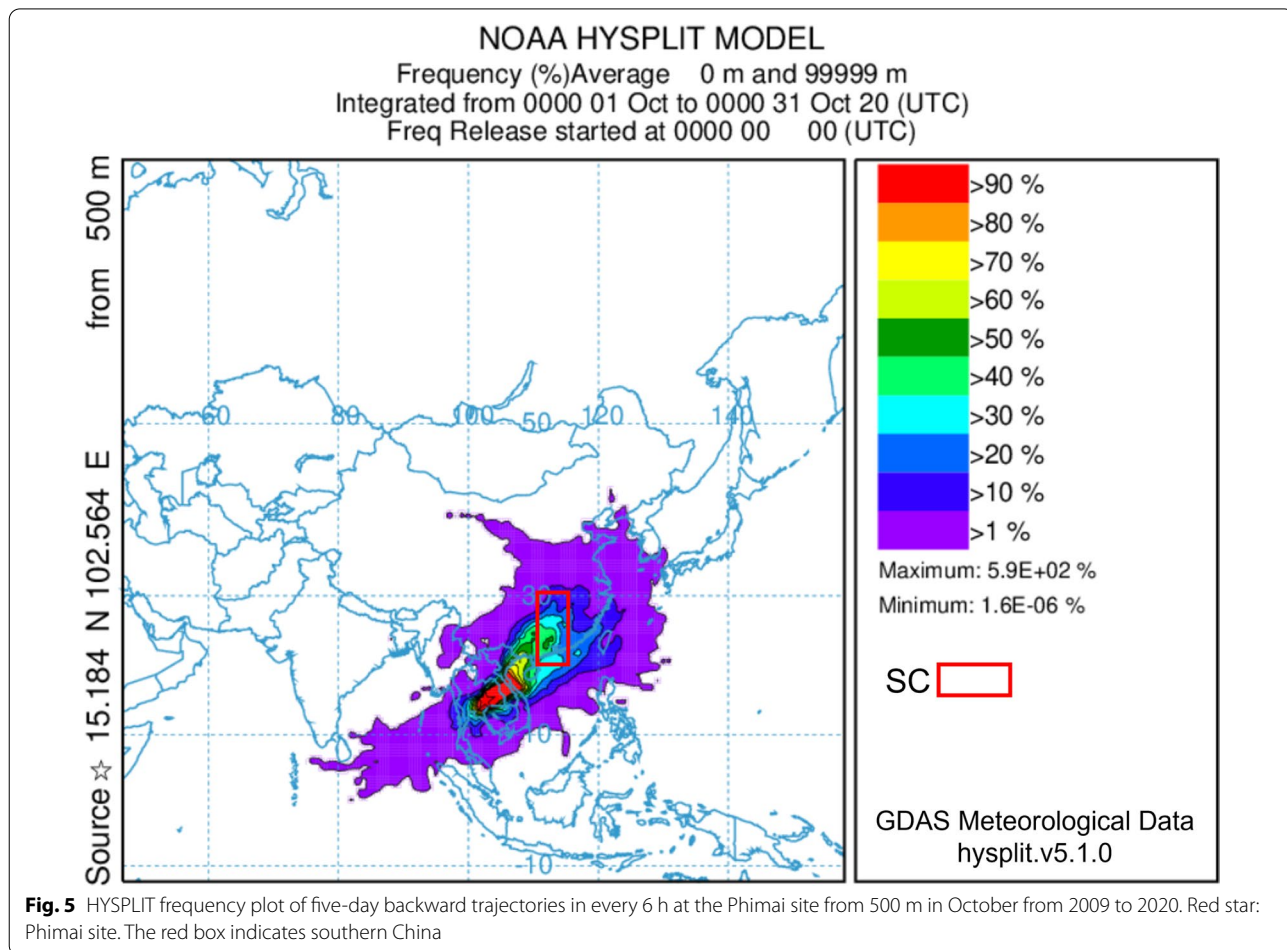


**Fig. 5** HYSPLIT frequency plot of five-day backward trajectories in every 6 h at the Phimai site from 500 m in October from 2009 to 2020. Red star: Phimai site. The red box indicates southern China



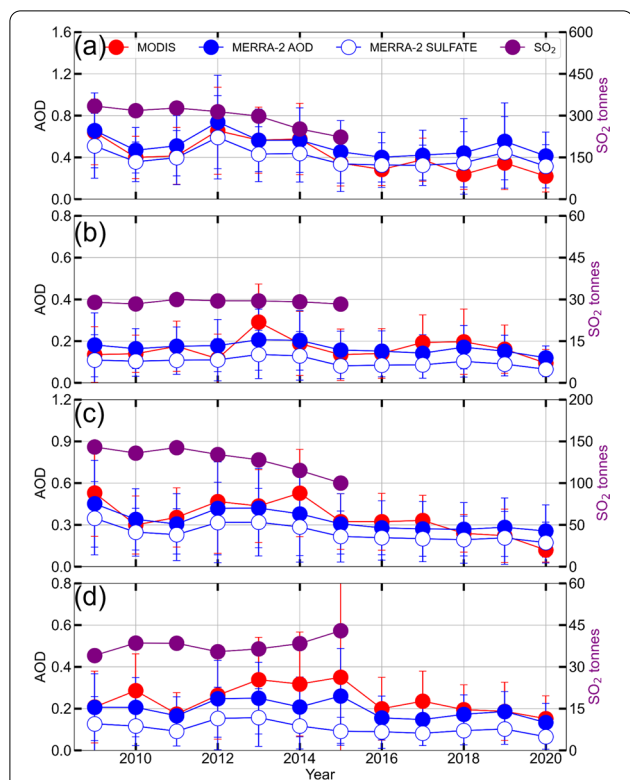


**Fig. 6** Total and sulfate AODs and SO<sub>2</sub> emissions in **a** Southern China, **b** NWIC, **c** NEIC and **d** SIC from 2009 to 2020. Error bar: standard deviation; blue closed and open plots: total and sulfate AOD, respectively; red plot: MODIS AOD; purple plot: SO<sub>2</sub> emissions [tonnes]

In ICP, MERRA-2 AOD was underestimated compared to AERONET data (RMBs of AOD tended to be less than 1) (Cho et al. 2019). Therefore, we applied case 2 correction to ICP that are similarly affected by BB. Table 2 lists the rates of change in the OC and sulfate AOD to total AOD ratios before and after the application of the case 2 correction in the dry season. Rates of change were calculated as  $(r_{after}/r_{before}) - 1$ , where  $r$  is the ratio of OC or sulfate AOD to the total AOD. In the active BB period (from January to March), the ratio of OC AOD to the total AOD after the

correction increased by more than 9%, whereas that of sulfate AOD to the total AOD decreased by up to 16%. Because OC aerosol is dominant in this period (Fig. 4), the impact of the correction may be substantial. In contrast, from October to December (no BB and sulfate dominance), there was no significant change in the sulfate AOD (< 10%). The rate of change was lowest in NEIC because of anthropogenic emissions. Therefore, the effect of corrections in this period is small.

Frequency analysis of five-day backward trajectories at Phimai in October from 2009 to 2020 showed a dominant trend in two wind directions (Fig. 5), indicating that the wind transitions from southwest to northeast due to monsoon (Sugimoto et al. 2008; Tsujimoto et al. 2018). AODs in NEIC and SIC were affected by the movement of air masses from China. The movement of (NH<sub>4</sub>)<sub>2</sub>SO<sub>4</sub>-rich air masses from East Asia was detected at Phimai through sampling and trajectory analyses (Tsuruta et al. 2008, 2009). On the basis of trajectory frequency analysis, areas northeast of NEIC with a frequency of 30% or more were defined as SC. In SC, which is a windward region with an anthropogenic aerosol source, AOD was more than 0.5 in October (Zhang et al. 2018), which is higher than that in NEIC and SIC. In Hanoi, a major city in NEIC located on the trajectory pathway to Phimai, the BC aerosol increases because of the circulation of pollutants from SC in October (Lasko et al. 2019). Therefore, AODs in NEIC and SIC increase because of pollutant circulation from China in October, which is driven by a change in the wind direction.

### 3.3 Trend analysis for October

It is suitable to investigate the impact of emissions from China in October because BB is inactive; thus, the contribution of anthropogenic aerosols is high. The total and sulfate AOD trends are shown in Fig. 6 and Table 3. The total and sulfate AODs decreased in all ICP regions. The decrease was highest in NEIC, followed by SIC and NWIC (− 4.40, − 3.00, and − 2.53% year<sup>−1</sup>, respectively). MODIS AOD showed similar trends. Therefore, the MERRA-2 dataset suggests that the decrease in AOD is consistent and mainly caused by sulfate AOD.

**Table 3** MERRA-2 AOD, sulfate AOD, MODIS AOD, and REAS SO<sub>2</sub> trends (% year<sup>−1</sup> [slope])

Region	MERRA-2		MODIS	REAS
	AOD	Sulfate AOD	AOD	SO <sub>2</sub>
SC	− 3.10 (− 0.0160)	− 3.01 (− 0.0121)	− 7.32 (− 0.0308)	− 6.00 (− 17.70)
NWIC	− 2.53 (− 0.0042)	− 3.38 (− 0.0034)	− 0.45 (− 0.0007)	− 0.11 (− 0.03)
NEIC	− 4.40 (− 0.0146)	− 5.05 (− 0.0124)	− 7.27 (− 0.0253)	− 5.17 (− 6.63)
SIC	− 3.00 (− 0.0058)	− 4.48 (− 0.0048)	− 2.72 (− 0.0066)	2.29 (0.87)

Next, we evaluated factors contributing to the decrease in the total and sulfate AODs in October. From 2010 to 2017, AOD in China decreased because of the environmental protection measures mandated by the Chinese government (Sun et al. 2019b). Trend analysis was performed in SC similar to that for ICP, as ICP is affected by transboundary transport from SC (Fig. 5). In this study, we used monthly SO<sub>2</sub> emission data from the Regional Emission inventory in Asia (REAS) version 3.2.1 (Kurokawa and Ohara, 2020). SO<sub>2</sub> is a precursor for sulfate aerosol, which is useful for identifying the sources of anthropogenic emissions. SO<sub>2</sub> emissions in NEIC and SC decreased by 6.00 and 5.17% year<sup>-1</sup>, respectively (Fig. 6). In contrast, they increased by 2.29% year<sup>-1</sup> in SIC and showed no significant change in NWIC. SO<sub>2</sub> emissions in SC decreased by 2.5 times compared to that in NEIC (−17.70 and −6.63 tonnes year<sup>-1</sup>, respectively), suggesting a significant effect on ICP. In SIC, despite the increase in SO<sub>2</sub> emissions, sulfate AOD decreased, which is attributed to the decrease in SO<sub>2</sub> emissions in SC and NEIC. These results indicate that the decrease in anthropogenic aerosols in SC could affect the downwind ICP.

#### 4 Conclusions

We conducted a spatiotemporal variation analysis in ICP using MERRA-2 aerosol datasets. The MERRA-2 datasets were validated using ground-based sky radiometers and MAX-DOAS at the SKYNET Phimai site in the central ICP. The MERRA-2 AOD, AAOD, and AEC at altitudes below 1 km were underestimated in the dry season, likely because the amounts of BB aerosols (OC and BC) near the ground were insufficient. OC AOD was dominant in the dry season, whereas sulfate AOD was high all year round. AOD significantly increased in October in both NEIC and SIC, corresponding to the increase in sulfate AOD from 2009 to 2020. Trajectory analysis revealed the movement of anthropogenic air masses from SC in October. AOD decreased in October NEIC and SIC (−4.40% and −3.00% year<sup>-1</sup>, respectively), and SO<sub>2</sub> emissions decreased in SC and NEIC (−17.70 and −6.63 tonnes year<sup>-1</sup>, respectively) but increased in SIC (0.87 tonnes year<sup>-1</sup>). Therefore, the improvement in the air quality in SC could improve the air quality in the downwind ICP in October because of the air transportation by northeasterly winds.

#### Abbreviations

ICP: Indochina Peninsula; BB: Biomass burning; MAX-DOAS: Multi-axis differential optical absorption spectroscopy; MERRA-2: Modern-Era Retrospective Analysis for Research and Applications, version 2; NWIC: Northwest Indochina Peninsula; NEIC: Northeast Indochina Peninsula; SIC: South Indochina Peninsula; SC: Southern China; OC: Organic carbon; BC: Black carbon; UV: Ultraviolet; AOD: Aerosol optical depth; SSA: Single scattering albedo; AAOD: Absorption aerosol optical depth; AE: Ångström exponent; AAE: Absorption

Ångström exponent; AEC: Aerosol extinction coefficient; ΔSCD: Differential slant column density; SR-CERES: Sky radiometer analysis package from center for environmental remote sensing; JM2: Japanese MAX-DOAS profile retrieval algorithm, version 2; AERONET: Aerosol robotic network; MODIS: Moderate-resolution imaging spectroradiometer; NASA: National Aeronautics and Space Administration; GEOS-5: Goddard Earth Observing System, version 5; GOCART: Goddard chemistry aerosol radiation and transport model; *R*: Pearson correlation coefficient; MAE: Mean absolute error; RMSE: Root-mean-square error; RMB: Relative mean bias; MFE: Mean fractional error; MFB: Mean fractional bias; IOA: Index of agreement; *M*: MERRA-2 datasets; *O*: Observation datasets.

#### Acknowledgements

This research was supported by the Environment Research and Technology Development Fund (JPMEERF20192001 and JPMEERF20215005) of the Environmental Restoration and Conservation Agency of Japan, JSPS KAKENHI (grant numbers JP20H04320, JP21K12227, JP22H03727, and JP22H05004), the JAXA 3rd research announcement on the Earth Observations (grant number 19RT000351), and the Virtual Laboratory (VL) project by the Ministry of Education, Culture, Sports, Science and Technology (MEXT), Japan. We are grateful to Mr. Ravi C. Govindaraju for providing us with MERRA-2 EXT data.

#### Author contributions

TO and HI designed the present study, performed observation and analysis, and wrote the paper, with support from all the authors. MM and AMS gave useful comments. All authors read and approved the final manuscript.

#### Funding

This research was supported by the Environment Research and Technology Development Fund (JPMEERF20192001 and JPMEERF20215005) of the Environmental Restoration and Conservation Agency of Japan, JSPS KAKENHI (Grant Numbers JP20H04320, JP21K12227, JP22H03727, and JP22H05004), the JAXA 3rd research announcement on the Earth Observations (Grant Number 19RT000351), and the Virtual Laboratory (VL) project by the Ministry of Education, Culture, Sports, Science and Technology (MEXT), Japan.

#### Availability of data and materials

The data are available upon request to the corresponding author (t.ohno.chiba@gmail.com).

#### Declarations

#### Competing interests

The authors declare that they have no competing interests.

#### Author details

<sup>1</sup>Center for Environmental Remote Sensing, Chiba University, 1-33 Yayoi-cho, Inage-Ku, Chiba 263-8522, Japan. <sup>2</sup>GRASP SAS, 3 avenue Louis Neel, 59260 Lezennes, Nord, France. <sup>3</sup>Present Address: DoerResearch Inc., 1-20-3 Matsusonochi, Mizuho-Ku, Nagoya, Aichi 467-0065, Japan. <sup>4</sup>NASA Goddard Space Flight Center, Greenbelt, MD, USA.

Received: 12 July 2022 Accepted: 31 October 2022

Published online: 12 November 2022

#### References

- Bond TC, Doherty SJ, Fahey DW, Forster PM, Berntsen T, DeAngelo BJ, Flanner MG, Ghan S, Kaercher B, Koch D, Kinne S, Kondo Y, Quinn PK, Sorooshian MC, Schultz MG, Schulz M, Venkataraman C, Zhang H, Zhang S, Bellouin N, Guttikunda SK, Hopke PK, Jacobson MZ, Kaiser JW, Klimont Z, Lohmann U, Schwarz JP, Shindell D, Storelvmo T, Warren SG, Zender CSJ (2013) Bounding the role of black carbon in the climate system: a scientific assessment. *J Geophys Res Atmos* 118:5380–5552. <https://doi.org/10.1002/jgrd.50171>
- Boylan JW, Russell AG (2006) PM and light extinction model performance metrics, goals, and criteria for three-dimensional air quality models. *Atmos Environ* 40:4946–4959. <https://doi.org/10.1016/j.atmosenv.2005.09.087>
- Brook RD, Rajagopalan S, Pope CA, Brook JR, Bhatnagar A, Diez-Roux AV, Holguin F, Hong Y, Luepker RV, Mittleman MA, Peters A, Siscovick D, Smith

- SC, Whitsel L, Kaufman JD (2010) Particulate matter air pollution and cardiovascular disease: an update to the scientific statement from the American heart association. *Circulation* 121:2331–2378. <https://doi.org/10.1161/CIR.0b013e3181dbee1>
- Brown H, Liu X, Feng Y, Jiang Y, Wu M, Lu Z, Wu C, Murphy S, Pokhrel R (2018) Radiative effect and climate impacts of brown carbon with the Community Atmosphere Model (CAM5). *Atmos Chem Phys* 18:17745–17768. <https://doi.org/10.5194/acp-18-17745-2018>
- Buchard V, da Silva AM, Randles CA, Colarco P, Ferrare R, Hair J, Hostetler C, Tackett J, Winker D (2016) Evaluation of the surface PM<sub>2.5</sub> in version 1 of the NASA MERRA aerosol reanalysis over the United States. *Atmos Environ* 125:100–111. <https://doi.org/10.1016/j.atmosenv.2015.11.004>
- Buchard V, Randles CA, da Silva AM, Darmenov A, Colarco PR, Govindaraju R, Ferrare R, Hair J, Beyersdorf AJ, Ziemba LD, Yu H (2017) The MERRA-2 aerosol reanalysis, 1980 onward. Part II: evaluation and case studies. *J Clim* 30(17):6851–6872. <https://doi.org/10.1175/JCLI-D-16-0613.1>
- Che H, Gui K, Xia X, Wang Y, Holben BN, Goloub P, Cuevas-Agulló E, Wang H, Zheng Y, Zhao H, Zhang X (2019) Large contribution of meteorological factors to inter-decadal changes in regional aerosol optical depth. *Atmos Chem Phys* 19:10497–10523. <https://doi.org/10.5194/acp-19-10497-2019>
- Chin M, Ginoux P, Kinne S, Torres O, Holben BN, Duncan BN, Martin RV, Logan JA, Higurashi A, Nakajima T (2002) Tropospheric aerosol optical thickness from the GOCART Model and comparisons with satellite and sun photometer measurements. *J Atmos Sci* 59(3):461–483. [https://doi.org/10.1175/1520-0469\(2002\)059%3c0461:TAOTFT%3e2.0.CO;2](https://doi.org/10.1175/1520-0469(2002)059%3c0461:TAOTFT%3e2.0.CO;2)
- Darmenov AS, da Silva AM (2015) The quick fire emissions dataset (QFED): Documentation of versions 2.1, 2.2 and 2.4. Technical Report Series on Global Modeling and Data Assimilation. NASA Tech Rep NASA/TM–2015–104606 38:212. <https://gmao.gsfc.nasa.gov/pubs/docs/Darmenov796.pdf>
- Dubovik O, Holben B, Eck TF, Smirnov A, Kaufman YJ, King MD, Tanré D, Slutsker I (2002) Variability of absorption and optical properties of key aerosol types observed in worldwide locations. *J Atmos Sci* 59(3):590–608. [https://doi.org/10.1175/1520-0469\(2002\)059%3c0590:VOAOP%3e2.0.CO;2](https://doi.org/10.1175/1520-0469(2002)059%3c0590:VOAOP%3e2.0.CO;2)
- Gelaro R, McCarty W, Suárez MJ, Todling R, Molod A, Takacs L, Randles CA, Darmenov A, Bosilovich MG, Reichle R, Wargan K, Coy L, Cullather R, Draper C, Akella S, Buchard V, Conaty A, da Silva AM, Gu W, Kim G, Koster R, Lucchesi R, Merkova D, Nielsen JE, Partyka G, Pawson S, Putman W, Rienecker M, Schubert SD, Sienkiewicz M, Zhao B (2017) The modern-era retrospective analysis for research and applications, version 2 (MERRA-2). *J Clim* 30(14):5419–5454. <https://doi.org/10.1175/JCLI-D-16-0758.1>
- Gueymard CA, Yang D (2020) Worldwide validation of CAMS and MERRA-2 reanalysis aerosol optical depth products using 15 years of AERONET observations. *Atmos Environ* 225:117216. <https://doi.org/10.1016/j.atmosenv.2019.117216>
- Hashimoto M, Nakajima T, Dubovik O, Campanelli M, Che H, Khatri P, Takamura T, Pandithurai G (2012) Development of a new data-processing method for SKYNET sky radiometer observations. *Atmos Meas Tech* 5:2723–2737. <https://doi.org/10.5194/amt-5-2723-2012>
- Hien PD, Bac VT, Thanh NTH (2004) PMF receptor modelling of fine and coarse PM<sub>10</sub> in air masses governing monsoon conditions in Hanoi, northern Vietnam. *Atmos Environ* 38:189–201. <https://doi.org/10.1016/j.atmosenv.2003.09.064>
- IPCC (2021) Summary for policymakers. In: Masson-Delmotte V, Zhai P, Pirani A, Connors SL, Péan C, Berger S, Caud N, Chen Y, Goldfarb L, Gomis MI, Huang M, Leitzell K, Lonnoy E, Matthews JBR, Maycock TK, Waterfield T, Yelekçi O, Yu R, and Zhou B (eds) *Climate change 2021: The physical science basis. Contribution of working group I to the sixth assessment report of the intergovernmental panel on climate change*. Cambridge University Press (In Press)
- Irie H, Kanaya Y, Akimoto H, Iwabuchi H, Shimizu A, Aoki K (2008) First retrieval of tropospheric aerosol profiles using MAX-DOAS and comparison with lidar and sky radiometer measurements. *Atmos Chem Phys* 8:341–350. <https://doi.org/10.5194/acp-8-341-2008>
- Irie H, Takashima H, Kanaya Y, Boersma KF, Gast L, Wittrock F, Brunner D, Zhou Y, Van Roozendaal M (2011) Eight-component retrievals from ground-based MAX-DOAS observations. *Atmos Meas Tech* 4:1027–1044. <https://doi.org/10.5194/amt-4-1027-2011>
- Irie H, Nakayama T, Shimizu A, Yamazaki A, Nagai T, Uchiyama A, Zaizen Y, Kagamitani S, Matsumi Y (2015) Evaluation of MAX-DOAS aerosol retrievals by coincident observations using CRDS, lidar, and sky radiometer in Tsukuba, Japan. *Atmos Meas Tech* 8:2775–2788. <https://doi.org/10.5194/amt-8-2775-2015>
- Irie H, Hoque HMS, Damiani A, Okamoto H, Fatmi AM, Khatri P, Takamura T, Jarupongsakul T (2019) Simultaneous observations by sky radiometer and MAX-DOAS for characterization of biomass burning plumes in central Thailand in January–April 2016. *Atmos Meas Tech* 12:599–606. <https://doi.org/10.5194/amt-12-599-2019>
- Kalita G, Kunchala RK, Fadnavis S, Kaskaoutis DG (2020) Long term variability of carbonaceous aerosols over Southeast Asia via reanalysis: association with changes in vegetation cover and biomass burning. *Atmos Res*. <https://doi.org/10.1016/j.atmosres.2020.105064>
- Khatri P, Takamura T (2009) An algorithm to screen cloud affected data for sky radiometer data analysis. *J Meteor Soc Jpn* 87:189–204. <https://doi.org/10.2151/jmsj.87.189>
- Kurokawa J, Ohara T (2020) Long-term historical trends in air pollutant emissions in Asia: Regional emission inventory in Asia (REAS) version 3. *Atmos Chem Phys* 20:12761–12793. <https://doi.org/10.5194/acp-20-12761-2020>
- Lasko K, Vadrevu KP, Nguyen TTN (2019) Correction: analysis of air pollution over Hanoi, Vietnam using multi-satellite and MERRA reanalysis datasets. *PLoS ONE* 14(3):e0214628. <https://doi.org/10.1371/journal.pone.0214628>
- Lave LB, Seskin EP (1970) Air pollution and human health. *Science* 169:723–733. <https://doi.org/10.1126/science.169.3947.723>
- Lee HH, Bar-Or RZ, Wang C (2017) Biomass burning aerosols and the low-visibility events in Southeast Asia. *Atmos Chem Phys* 17:965–980. <https://doi.org/10.5194/acp-17-965-2017>
- Levy RC, Remer LA, Dubovik O (2007) Global aerosol optical properties and application to moderate resolution imaging spectroradiometer aerosol retrieval over land. *J Geophys Res* 112:D13210. <https://doi.org/10.1029/2006JD007815>
- Li H, Zhang Q, Zhang Q, Chen C, Wang L, Wei Z, Zhou S, Parworth C, Zheng B, Canonaco F, Prévôt ASH, Chen P, Zhang H, Wallington TJ, He K (2017a) Wintertime aerosol chemistry and haze evolution in an extremely polluted city of the North China Plain: significant contribution from coal and biomass combustion. *Atmos Chem Phys* 17:4751–4768. <https://doi.org/10.5194/acp-17-4751-2017>
- Li Z, Guo J, Ding A, Liao H, Liu J, Sun Y, Zhu B (2017b) Aerosol and boundary-layer interactions and impact on air quality. *Natl Sci Rev* 4:810–833. <https://doi.org/10.1093/nsr/nwx117>
- Lin G, Penner JE, Flanner MG, Sillman S, Xu L, Zhou C (2014) Radiative forcing of organic aerosol in the atmosphere and on snow: effects of SOA and brown carbon. *J Geophys Res Atmos* 119:7453–7476. <https://doi.org/10.1002/2013JD021186>
- Mok J, Krotkov NA, Arola A, Torres O, Jethva H, Andrade M, Labow G, Eck TF, Li Z, Dickerson RR, Stenchikov GL, Osipov S, Ren X (2016) Impacts of brown carbon from biomass burning on surface UV and ozone photochemistry in the Amazon Basin. *Sci Rep* 6:36940. <https://doi.org/10.1038/srep36940>
- Mok J, Krotkov NA, Torres O, Jethva H, Li Z, Kim J, Koo J-H, Go S, Irie H, Labow G, Eck TF, Holben BN, Herman J, Loughman RP, Spinei E, Lee SS, Khatri P, Campanelli M (2018) Comparisons of spectral aerosol single scattering albedo in Seoul, South Korea. *Atmos Meas Tech* 11:2295–2311. <https://doi.org/10.5194/amt-11-2295-2018>
- Nakajima T, Tonna G, Rao R, Boi P, Kaufman Y, Holben B (1996) Use of sky brightness measurements from ground for remote sensing of particulate polydispersions. *Appl Opt* 35:2672–2686
- Nakajima T, Campanelli M, Che H, Estellés V, Irie H, Kim S-W, Kim J, Liu D, Nishizawa T, Pandithurai G, Soni VK, Thana B, Tugjurn N-U, Aoki K, Go S, Hashimoto M, Higurashi A, Kazadzis S, Khatri P, Kouremeti N, Kudo R, Marengo F, Momoi M, Ningombam SS, Ryder CL, Uchiyama A, Yamazaki A (2020) An overview of and issues with sky radiometer technology and SKYNET. *Atmos Meas Tech* 13:4195–4218. <https://doi.org/10.5194/amt-13-4195-2020>
- Proestakis E, Amiridis V, Marinou E, Georgoulas AK, Solomos S, Kazadzis S, Chimit J, Che H, Alexandri G, Biniotoglou I, Daskalopoulou V, Kourtidis KA, de Leeuw G, van der ARJ (2018) Nine-year spatial and temporal evolution of desert dust aerosols over South and East Asia as revealed by CALIOP. *Atmos Chem Phys* 18:1337–1362. doi:10.5194/acp-18-1337-2018.
- Ramanathan V, Carmichael G (2008) Global and regional climate changes due to black carbon. *Nat Geosci* 1:221–227. <https://doi.org/10.1038/ngeo156>
- Randles CA, da Silva AM, Buchard V, Colarco PR, Darmenov A, Govindaraju R, Smirnov A, Holben B, Ferrare R, Hair J, Shinozuka Y, Flynn CJ (2017) The MERRA-2 aerosol reanalysis, 1980 onward. Part I: system description and

- data assimilation evaluation. *J Clim* 30(17):6823–6850. <https://doi.org/10.1175/JCLI-D-16-0609.1>
- Randles CA, da Silva AM, Buchard V, Darnenov A, Colarco PR, Aquila V, Bian H, Nowottnick EP, Pan X, Smirnov A, Yu H, and Govindaraju R (2016) The MERRA-2 aerosol assimilation. NASA TM-2016–104606, vol 45, NASA Global Modeling and Assimilation Office, pp 132. <https://gmao.gsfc.nasa.gov/reanalysis/MERRA-2/docs/>. Accessed 19 May 2022
- Rodgers CD (2000) Inverse method for atmospheric sounding. World Science, Singapore
- Shi H, Xiao Z, Zhan X, Ma H, Tian X (2019) Evaluation of MODIS and two reanalysis aerosol optical depth products over aeronet sites. *Atmos Res* 220:75–80. <https://doi.org/10.1016/j.atmosres.2019.01.009>
- Sugimoto N, Shimizu A, Nishizawa T, Matsui I, Jin Y, Khatri P, Irie H, Takamura T, Aoki K, Thana B (2015) Aerosol characteristics in Phimai, Thailand determined by continuous observation with a polarization sensitive Mie-Raman lidar and a sky radiometer. *Environ Res Lett* 10(6):065003. <https://doi.org/10.1088/1748-9326/10/6/065003>
- Sun E, Che H, Xu X, Wang Z, Lu C, Gui K, Zhao H, Zheng Y, Wang Y, Wang H, Sun T, Liang Y, Li X, Sheng Z, An L, Zhang X, Shi G (2019a) Variation in MERRA-2 aerosol optical depth over the Yangtze river delta from 1980 to 2016. *Theor Appl Climatol* 136:363–375. <https://doi.org/10.1007/s00704-018-2490-9>
- Sun E, Xu X, Che H, Tang Z, Gui K, An L, Lu C, Shi G (2019b) Variation in MERRA-2 aerosol optical depth and absorption aerosol optical depth over China from 1980 to 2017. *J Atmos Sol-Terr Phys* 186:8–19. <https://doi.org/10.1016/j.jastp.2019.01.019>
- Tsujimoto K, Ohta T, Aida K, Tamakawa K, Im MS (2018) Diurnal pattern of rainfall in Cambodia: its regional characteristics and local circulation. *Prog Earth Planet Sci* 5:1–18. <https://doi.org/10.1186/s40645-018-0192-7>
- Tsuruta H, Chotpitayasunon J, Thana B, Khatri P, Takamura T, Sudo S, Yonemura S, Sera K, Saitoh Y, Shirasuna Y, Hirano K, Hayasaka T, Nakajima T (2008) Chemical characterization of atmospheric aerosols measured at Phimai, Thailand. *NMCC Ann Rep* 15:75–86 (**in Japanese**)
- Tsuruta H, Chotpitayasunon J, Thana B, Takamura T, Sudo S, Yonemura S, Sera K, Saitoh Y, Shirasuna Y, Hirano K, Hayasaka T, Nakajima T (2009) Chemical characterization of atmospheric aerosols at Phimai, Thailand: II. Contribution of fossil fuel combustion, biomass burning, and soil dust. *NMCC Ann Rep* 16:152–162 (**in Japanese**)
- Uchiyama A, Matsunaga T, Yamazaki A (2018) The instrument constant of sky radiometers (POM-02)—Part 2: solid view angle. *Atmos Meas Tech* 11:5389–5402. <https://doi.org/10.5194/amt-11-5389-2018>
- Vadrevu KP, Lasko K, Giglio L, Justice C (2015) Vegetation fires, absorbing aerosols and smoke plume characteristics in diverse biomass burning regions of Asia. *Environ Res Lett* 10:105003. <https://doi.org/10.1088/1748-9326/10/10/105003>
- van der Werf GR, Randerson JT, Giglio L, Collatz GJ, Kasibhatla PS, Arellano AF (2006) Interannual variability in global biomass burning emissions from 1997 to 2004. *Atmos Chem Phys* 6:3423–3441. <https://doi.org/10.5194/acp-6-3423-2006>
- van der Werf GR, Randerson JT, Giglio L, van Leeuwen TT, Chen Y, Rogers BM, Mu M, van Marle MJE, Morton DC, Collatz GJ, Yokelson RJ, Kasibhatla PS (2017) Global fire emissions estimates during 1997–2016. *Earth Syst Sci Data* 9:697–720. <https://doi.org/10.5194/essd-9-697-2017>
- Wang X, Heald CL, Ridley DA, Schwarz JP, Spackman JR, Perring AE, Coe H, Liu D, Clarke AD (2014) Exploiting simultaneous observational constraints on mass and absorption to estimate the global direct radiative forcing of black carbon and brown carbon. *Atmos Chem Phys* 14:10989–11010. <https://doi.org/10.5194/acp-14-10989-2014>
- Wang SH, Welton EJ, Holben BN, Tsay SC, Lin NH, Giles D, Stewart SA, Janjai S, Nguyen XA, Hsiao TC, Chen WN, Lin TH, Buntoung S, Chantara S, Wiriya W (2015) Vertical distribution and columnar optical properties of springtime biomass-burning aerosols over Northern Indochina during 2014 7-SEAS campaign. *Aerosol Air Qual Res* 15:2037–2050. <https://doi.org/10.4209/aaqr.2015.05.0310>
- Wei J, Li Z, Peng Y, Sun L (2019) MODIS collection 6.1 aerosol optical depth products over land and ocean: validation and comparison. *Atmos Environ* 201:428–440. <https://doi.org/10.1016/j.atmosenv.2018.12.004>
- Wiedinmyer C, Akagi SK, Yokelson RJ, Emmons L, Al-Saadi JA, Orlando JJ, Soja AJ (2011) The Fire Inventory from NCAR (FINN): a high resolution global model to estimate the emissions from open burning. *Geosci Model Dev* 4:625–641. <https://doi.org/10.5194/gmd-4-625-2011>
- Willmott CJ (1981) On the validation of models. *Phys Geogr* 2:184–194. <https://doi.org/10.1002/joc.2419>
- Yadav IC, Devi NL, Li J, Syed JH, Zhang G, Watanabe H (2017) Biomass burning in Indo-China peninsula and its impacts on regional air quality and global climate change—a review. *Environ Pollut* 227:414–427. <https://doi.org/10.1016/j.envpol.2017.04.085>
- Yin S, Wang X, Zhang X, Guo M, Miura M, Xiao Y (2019) Influence of biomass burning on local air pollution in mainland Southeast Asia from 2001 to 2016. *Environ Pollut* 254:112949. <https://doi.org/10.1016/j.envpol.2019.07.117>
- Yumimoto K, Tanaka TY, Oshima N, Maki T (2017) JRAero: the Japanese reanalysis for aerosol v1.0. *Geosci Model Dev* 10:3225–3253. <https://doi.org/10.5194/gmd-10-3225-2017>
- Zhang M, Wang Y, Ma YY, Wang LC, Gong W, Liu BM (2018) Spatial distribution and temporal variation of aerosol optical depth and radiative effect in South China and its adjacent area. *Atmos Environ* 188:120–128. <https://doi.org/10.1016/j.atmosenv.2018.06.028>

## Publisher's Note

Springer Nature remains neutral with regard to jurisdictional claims in published maps and institutional affiliations.

Submit your manuscript to a SpringerOpen® journal and benefit from:

- Convenient online submission
- Rigorous peer review
- Open access: articles freely available online
- High visibility within the field
- Retaining the copyright to your article

Submit your next manuscript at ► [springeropen.com](https://www.springeropen.com)